

Exploring non-singular black holes in gravitational perturbations

Hang Liu,^{1,2} Chao Zhang,³ Yungui Gong,³ Bin Wang,^{4,2,*} and Anzhong Wang⁵

¹*School of Physics and Astronomy,*

Shanghai Jiao Tong University, Shanghai 200240, China

²*School of Aeronautics and Astronautics,*

Shanghai Jiao Tong University, Shanghai 200240, China

³*School of Physics, Huazhong University of Science
and Technology, Wuhan, Hubei 430074, China*

⁴*Center for Gravitation and Cosmology,*

Yangzhou University, Yangzhou 225009, China.

⁵*GCAP-CASPER, Physics Department,*

Baylor University, Waco, TX, 76798-7316, USA

Abstract

We calculate gravitational perturbation quasinormal modes (QNMs) of non-singular Bardeen black holes (BHs) and singularity-free BHs in conformal gravity and examine their spectra in wave dynamics comparing with standard BHs in general relativity. After testing the validity of the approximate signal-to-noise ratio (SNR) calculation for different space based interferometers, we discuss the SNR of non-singular BHs in single-mode gravitational waveform detections in LISA, TianQin and TaiJi. We explore the impact of the Bardeen parameter and the conformal factor on the behavior of the SNR and find that in comparison with the standard Schwarzschild BHs, the increase of non-singular parameters leads to higher SNR for more massive non-singular BHs. We also examine the effect of the galactic confusion noise on the SNR and find that a dip appears in SNR due to such noise. For non-singular BHs, with the increase of the non-singular parameters the dip emerges for more massive BHs. Imprints of non-singular BHs on peaks and dips in SNR imply that non-singular BHs are likely to be distinguished from the standard Schwarzschild BHs when BHs are sufficient massive. The detections of non-singular BHs are expected to be realized more likely by LISA or TaiJi.

* Corresponding Author: Bin Wang, wang_b@sjtu.edu.cn

I. INTRODUCTION

Gravitational waves (GWs) were predicted by Einstein's general relativity (GR) a century ago and since then huge amount of effort has been put into investigating the existence of GWs and thereby testing GR. Recently, the first and by far the strongest GW event GW150914 was detected by LIGO Scientific Collaboration and Virgo Collaboration [1]. More detections of GWs [2–7] have been reported afterwards. The landmark detection of GWs ended the era of a single electromagnetic wave channel observation of our universe. Successful detections of GWs announced the dawn of multi-messenger astronomy with GW as a new probe to study our universe.

The ground based interferometers (such as LIGO) inevitably suffer from the gravity gradient noise and seismic noise which lead to the limitation that the detection of GWs with frequencies lower than 10Hz is extremely challenging. However, it is of great significance to probe GWs in lower frequency bands because a large number of GW sources containing rich physics are expected to fall in the frequency bands from millihertz to hertz [8]. Among these sources, the mergers of massive black hole (MBH) binaries with mass between $10^3 M_\odot$ and $10^7 M_\odot$ are expected to happen frequently [9–11], although there is no conclusive evidence yet. The existence of MBHs has been confirmed in the center of galaxies, for example a black hole named Sagittarius A* with mass about $4 \times 10^6 M_\odot$ was discovered in the center of our Milky Way [12]. To detect GWs from intermediate and super massive sources, we have to move our detectors to space. Laser Interferometer Space Antenna (LISA) [13], TaiJi [14] and TianQin [15] are space based detectors to probe GWs with frequencies in the millihertz to hertz band.

Scientifically detecting GWs in space can disclose more physics of gravity. For the compact binaries, LIGO detected GW emission from the merger of binary neutron stars (BNS) (e.g. GW170817 [7]). The characteristic of BNS was confirmed and the BNS was distinguished from the merger of binary black holes (BBHs) with the help of the electromagnetic observation (e.g. gamma-ray burst [16, 17] and kilonova [18–23]). However the electromagnetic signal of BNS can be too weak to be detected provided that the initial BNS are far away or initial BNS are massive and collapse into black holes (BHs) [24–26] leaving negligible matter outside. It is expected that space based GW detectors can help uncover the tidal deformability in the binary system, whether it is zero or not [27] can serve to determine the

binary system being BBH or BNS. This signature can help understand better the galactic compact binaries. In addition, the quantum effect arising from the quantum correction to classical gravity theory around black hole event horizons can be encoded in GWs. It was argued that such quantum effect can be detected through the observation of GW echoes [28, 29]. The evidence for the echoes in GWs was disclosed in the LIGO observations [30]. Echo promises a new way to probe the supersized BHs in distant galaxies. There will be space based GW detectors to watch out for these binary giants' binge, which can shed further light on the quantum nature of gravity. The waveforms of GWs detected by ground-based detectors [1–6] successfully confirmed GR in the nonlinear and strong-field regimes. However, we know that GR is not complete, and in particular it is plagued with the singularity problem, the non-renormalization problem and has difficulties in understanding the universe at very large scales. These provide the motivations for conceiving modified theories of gravity. Whether the meddling with GR can produce GWs to be detected by ground based or space based detectors is an interesting question to be studied.

In this work we will concentrate on the study of an alternative theory of GR to accommodate singularity free black hole solutions to avoid the singularity problem in GR. The existence of singularities in the solutions to Einstein's field equations has been a longstanding problem. Hawking and Penrose proved a singularity theorem [31] which states that the singularity is unavoidable if GR holds and certain energy conditions are satisfied. An idea considering the quantum effect of gravity was proposed to eliminate singularities. In the vicinity of the singularity the curvature and energy density is so huge that the spacetime is strongly bended and the quantum nature of gravity dominates, while the classical GR description turns out to be inaccurate. Following this idea some attempts have been made [32–41] to alleviate the singularity problem although a consistent quantum theory of gravity is still absent so far. To cure the shortcoming of GR at infrared and ultraviolet scales, a wide class of modified theories of gravity has been constructed with the purpose of addressing conceptual and experimental problems emerged in the fundamental physics and providing at least an effective description of quantum gravity [42]. Considering the non-physical characteristics of singularities, it is natural to find non-singular solutions to Einstein's equations. The first non-singular black hole solution was found by Bardeen and it was later revealed that such a non-singular solution could be regarded as the gravitational collapse of a magnetic monopole with nonlinear electromagnetic energy-momentum tensor playing the role

of the source term in field equations [43]. In the conformal gravity frame, the black hole singularity could be removed under conformal transformations by taking advantage of the conformal symmetry of the spacetime [44–50]. The suitable conformal transformations can result in convergent curvature at coordinate $r = 0$ which usually corresponds to a singularity with divergent curvature in GR. In this sense, the spacetime singularity seems like an artifact under different choices of conformal gauges, just like the coordinate singularity at horizons which can be removed by proper coordinate transformations in GR. Because of the singularity-free feature of such non-singular BHs, it is reasonable to regard them as the realistic consequence of gravitational collapse of matter fields instead of the usual BHs with non-physical singularities.

It is of great interest to study the wave dynamics of such non-singular BHs and distinguish them from black hole solutions in GR. The study of wave dynamics outside BHs has been an intriguing subject for the last few decades (for recent review, see for example [51]). A static observer outside a black hole can indicate successive stages of the wave evolution. After the initial pulse, the gravitational field outside the black hole experiences a quasinormal ringing, which describes the damped oscillations under perturbations in the surrounding geometry of a black hole with frequencies and damping times of the oscillations entirely fixed by the black hole parameters. The quasinormal mode (QNM) is believed as a unique fingerprint to directly identify the black hole existence and distinguish different black hole solutions. We will employ the 13-th order WKB method with averaging of the Pade approximations suggested first in [52] to compute the QNM of non-singular BHs and compare it with the result of wave dynamics in usual BHs in GR. Since the numerical method we apply here has very high accuracy [53], we expect to find the special signatures of non-singular BHs in the wave dynamics.

The detection of QNMs can be realized through gravitational wave observations. From the observational point of view, we can calculate the signal-to-noise ratio (SNR) from the ringdown signals of GWs originated from the gravitational perturbations around BHs. Thus based on the precise QNM spectrum, we can obtain the SNR in GW observations. Different imprints in QNMs caused by different black hole configurations can be reflected in behaviors of the SNR. In order to distinguish different black hole solutions through the study of black hole spectroscopy, we require large SNR in the black hole ringdown phase. It was pointed out in [54, 55] that to resolve either the frequencies or damping time of fundamental mode

($n = 0$) from the first overtone ($n' = 1$) with the same angular dependence ($l = l', m = m'$), the critical value ρ_{cri} of SNR is required to be around $\rho_{cri} \simeq 100$, while to resolve both the frequencies and damping time typically requires $\rho_{cri} \simeq 1000$. The large SNR can serve as a smoking gun in GW observations to identify the existence of non-singular black hole solutions in alternative theories of gravity. In the following discussion, we will not only examine the SNR in LISA, but also extend the calculation of SNR to other space based GW observations, such as TaiJi and TianQin, to check the feasibility of testing the existence of non-singular BHs.

The organization of the paper is as follows. In Section II, we introduce the calculation of SNR for single-mode waveform detections. In Section III, we calculate the QNMs and the SNR for non-singular BHs in conformal gravity. In Section IV, we generalize such calculations to the case for non-singular Bardeen BHs. Finally in the last section we present our main conclusions. In Appendix A, we prove that the approximate formula in the SNR calculation developed in the context of LISA is general and can be applied to TaiJi and TianQin observations within acceptable errors.

II. THE SNR FOR SINGLE-MODE WAVEFORM

In this section, we give a brief review on how to calculate the SNR for a single-mode wave detection. The basic idea was proposed in [54] for LISA and we generalize the method to discuss the SNR for Tianqin and TaiJi.

The gravitational waveform composed of cross component h_{\times} and plus component h_{+} emitting from a perturbed black hole (or from the distorted final black hole merging from supermassive black hole pairs) can be expressed as

$$h_{+} + ih_{\times} = -\frac{2}{r^4} \int_{-\infty}^{+\infty} \frac{d\omega}{\omega^2} e^{i\omega t} \sum_{lm} S_{lm}(\iota, \beta) R_{lm\omega}(r), \quad (1)$$

where $R_{lm\omega}(r)$ is the radial Teukolsky function [56] with the approximation $R_{lm\omega}(r) \sim r^3 e^{-i\omega r} Z_{lm\omega}^{out}$ when $r \rightarrow \infty$. $Z_{lm\omega}^{out}$ is a complex amplitude. Now we assume that the gravitational waveform can be written as a formal QNM expansion and consider that the QNMs of the Schwarzschild and Kerr BHs always exist in pairs which should be included in the

waveform expansion. In this way we have

$$\begin{aligned}
h_+ + ih_\times &= \frac{1}{r} \sum_{lmn} \left\{ e^{i\omega_{lmn}t} e^{-t/\tau_{lmn}} S_{lmn}(\iota, \beta) Z_{lmn}^{out} + e^{i\omega'_{lmn}t} e^{-t/\tau'_{lmn}} S'_{lmn}(\iota, \beta) Z_{lmn}'^{out} \right\} \\
&= \frac{M}{r} \sum_{lmn} \left\{ \mathcal{A}_{lmn} e^{i(\omega_{lmn}t + \phi_{lmn})} e^{-t/\tau_{lmn}} S_{lmn}(\iota, \beta) + \right. \\
&\quad \left. \mathcal{A}'_{lmn} e^{i(-\omega_{lmn}t + \phi'_{lmn})} e^{-t/\tau_{lmn}} S_{lmn}^*(\iota, \beta) \right\}, \tag{2}
\end{aligned}$$

where we have rewritten the complex Z_{lmn}^{out} in terms of a real amplitude \mathcal{A}_{lmn} and a real phase ϕ_{lmn} , and we factor out the black hole mass M by $Z_{lmn}^{out} = M \mathcal{A}_{lmn} e^{i\phi_{lmn}}$. In the above expansion, $S_{lm}(\iota, \beta)$ stands for spin weighted spheroidal harmonics whose complex conjugate is denoted by $S_{lmn}^*(\iota, \beta)$, ι and β are angular variables, and l, m are indices analogous to those for standard spherical harmonics corresponding to a particular case of $S_{lmn}(\iota, \beta)$ in which both the perturbation field and black hole spin are zero, n denotes the overtone number. Note that we have the complex QNM frequency $\omega = \omega_{lmn} + i/\tau_{lmn}$, where the real part denotes the oscillation frequency $\omega_{lmn} = 2\pi f_{lmn}$ and the imaginary part τ_{lmn} is the damping time of the perturbation oscillation. For a single given mode labeled by (l, m, n) , the real waveform measured at the detector can be expressed as a linear superposition of h_+ and h_\times

$$h_+ = \frac{M}{r} \Re \left[\mathcal{A}_{lmn}^+ e^{i(\omega_{lmn}t + \phi_{lmn}^+)} e^{-t/\tau_{lmn}} S_{lmn}(\iota, \beta) \right], \tag{3a}$$

$$h_\times = \frac{M}{r} \Im \left[\mathcal{A}_{lmn}^\times e^{i(\omega_{lmn}t + \phi_{lmn}^\times)} e^{-t/\tau_{lmn}} S_{lmn}(\iota, \beta) \right], \tag{3b}$$

in which we have the relation $\mathcal{A}_{lmn}^{+, \times} e^{i\phi_{lmn}^{+, \times}} = \mathcal{A}_{lmn} e^{i\phi_{lmn}} \pm \mathcal{A}'_{lmn} e^{-i\phi'_{lmn}}$, where the signs $+(-)$ correspond to the $+(\times)$ polarizations respectively. The waveform h detected by a detector is given by

$$h = h_+ F_+(\theta_S, \phi_S, \psi_S, f) + h_\times F_\times(\theta_S, \phi_S, \psi_S, f), \tag{4}$$

where $F_{+, \times}$ are frequency dependent pattern functions (response functions) depending on the orientation ψ_S of the detector and the direction (θ_S, ϕ_S) of the source. For LIGO (in the long wavelength limit), we have

$$F_+ = \frac{1}{2} (1 + \cos^2 \theta_S) \cos 2\phi_S \cos 2\psi_S - \cos \theta_S \sin 2\phi_S \sin 2\psi_S, \tag{5a}$$

$$F_\times = \frac{1}{2} (1 + \cos^2 \theta_S) \sin 2\phi_S \cos 2\psi_S + \cos \theta_S \sin 2\phi_S \cos 2\psi_S, \tag{5b}$$

which are independent of the frequency. The sky and polarization averaged SNR is [54, 57],

$$\rho^2 = 4 \int_0^\infty \frac{\langle \tilde{h}^*(f) \tilde{h}(f) \rangle}{S_N(f)} df = 4 \int_0^\infty \frac{|\tilde{h}_+|^2 + |\tilde{h}_\times|^2}{S_n(f)} df, \quad (6a)$$

$$S_n(f) = \frac{S_N(f)}{\mathcal{R}(f)}, \quad (6b)$$

$$\mathcal{R}(f) = \langle |F_+(f)|^2 \rangle = \langle |F_\times(f)|^2 \rangle, \quad (6c)$$

where $\tilde{h}(f)$ is the Fourier transform of the waveform, $S_N(f)$ is the noise spectral density of the detector, $S_n(f)$ is the detector sensitivity, $\mathcal{R}(f)$ is the sky/polarization averaged response function. Especially, the response function \mathcal{R} in the low frequency limit is

$$\mathcal{R} = \frac{1}{32} \int_{-1}^1 (1 + 6x^2 + x^4) dx = \frac{1}{5}, \quad (7)$$

while the full expressions of $F_+(f)$ and $F_\times(f)$ for LISA, TianQin and TaiJi are much more complicated and can be found in [58, 59]. We perform the Fourier transform of the waveform by using the relation

$$\int_{-\infty}^{\infty} e^{i\omega t} (e^{\pm i\omega_{lmn}t - |t|/\tau_{lmn}}) dt = \frac{2/\tau_{lmn}}{(1/\tau_{lmn})^2 + (\omega \pm \omega_{lmn})^2} \equiv 2b_\pm. \quad (8)$$

Based on Eq. (8) we can easily work out the Fourier transform of the plus and cross components,

$$\tilde{h}_+ = \frac{1}{\sqrt{2}} \frac{M}{r} \mathcal{A}_{lmn}^+ \left[e^{i\phi_{lmn}^+} S_{lmn} b_+ + e^{-i\phi_{lmn}^+} S_{lmn}^* b_- \right], \quad (9a)$$

$$\tilde{h}_\times = -\frac{1}{\sqrt{2}} \frac{iM}{r} \mathcal{A}_{lmn}^\times \left[e^{i\phi_{lmn}^\times} S_{lmn} b_+ - e^{-i\phi_{lmn}^\times} S_{lmn}^* b_- \right]. \quad (9b)$$

We add a correction factor $1/\sqrt{2}$ to serve as a compensation in amplitude because we are using the FH convention (developed by Flanagan and Hughes [60]) to calculate the SNR. In the FH convention, the waveform for $t < 0$ is assumed to be identical to waveform for $t > 0$ and therefore we can replace the decay factor $e^{-t/\tau_{lmn}}$ with $e^{-|t|/\tau_{lmn}}$ in the Fourier transform such that a compensation is needed for the doubling. Then we can insert Eq. (9) into Eq. (6a) and do the integration to calculate SNR. However, as described in [54], a simple analytical formula of SNR can be derived by making some approximations in the calculation. In this way, we have the SNR expression as [54],

$$\rho_{FH} = \frac{1.31681 \times 10^4}{\mathcal{F}_{lmn}} \left(\frac{\epsilon_{rd}}{0.03} \right)^{\frac{1}{2}} \left(\frac{(1+z)M}{10^6 M_\odot} \right)^{\frac{3}{2}} \left(\frac{1 \text{ Gpc}}{D_L(z)} \right) \left(\frac{S_0}{S_n(f_{lmn})} \right)^{\frac{1}{2}} \frac{2Q_{lmn}}{\sqrt{1 + 4Q_{lmn}^2}}, \quad (10)$$

where $S_0 = 1.59 \times 10^{-41} \text{Hz}^{-1}$, \mathcal{F}_{lmn} is the dimensionless frequency defined by $\mathcal{F}_{lmn} = M\omega_{lmn}$, ϵ_{rd} is the radiation efficiency, M_\odot is the solar mass and M is the black hole (source) mass, Q_{lmn} is a dimensionless quality factor of QNMs defined by

$$Q_{lmn} = \pi f_{lmn} \tau_{lmn} = \frac{1}{2} \omega_{lmn} \tau_{lmn}, \quad (11)$$

and $D_L(z)$ is the luminosity distance which can be expressed as a function of cosmological redshift z of the source in the standard flat Λ CDM cosmological model as

$$D_L(z) = \frac{1+z}{H_0} \int_0^z \frac{dz'}{\sqrt{\Omega_M(1+z')^3 + \Omega_\Lambda}}. \quad (12)$$

We shall take the matter density $\Omega_M = 0.32$, the dark energy density $\Omega_\Lambda = 0.68$ and the Hubble constant $H_0 = 67 \text{ km s}^{-1} \text{ Mpc}^{-1}$. Eq. (10) was derived in the context of LISA by making some approximations such as $S_{lmn} \simeq \Re(S_{lmn})$ and large Q_{lmn} limit. We will show that these approximations and the derivation steps of Eq. (10) are not dependent on specific interferometric detectors, therefore Eq. (10) could be applied to other space based detectors such as TianQin and TaiJi. We will discuss the generality of the approximate SNR formula Eq. (10) in more details in Appendix A, and show that this formula is applicable to TianQin and TaiJi.

For the calculation of SNR, we will adopt the following noise and response functions for all three space based detectors [61]

$$S_N(f) = \frac{4S_a}{(2\pi f)^4 L^2} \left(1 + \frac{10^{-4} \text{Hz}}{f} \right) + \frac{S_x}{L^2}, \quad (13a)$$

$$\mathcal{R}(f) = \frac{3}{10} \left[1 + 0.6 \left(\frac{f}{f_*} \right)^2 \right]^{-1}, \quad (13b)$$

in which L is the detector arm length and $f_* = c/(2\pi L)$ is the transfer frequency, S_a is the acceleration noise and S_x is the position noise of the instruments, and we list these parameters for three detectors in Table. I.

In addition to the noise of the detectors, an effective noise can be generated by the galactic binaries. For LISA, the galactic noise can be well fitted as [57, 62]

$$S_c(f) = A f^{-7/3} e^{-f^\alpha + \beta f \sin(\kappa f)} [1 + \tanh(\gamma(f_k - f))] \text{Hz}^{-1}, \quad (14)$$

and the total sensitivity can be obtained by adding $S_c(f)$ to $S_n(f)$. The effects of the galactic noise on the SNR for LISA will be discussed later, and the parameters we are going

	LISA	TianQin	TaiJi
L	$2.5 \times 10^9 \text{m}$	$\sqrt{3} \times 10^8 \text{m}$	$3 \times 10^9 \text{m}$
$\sqrt{S_a}$	$3 \times 10^{-15} \text{ms}^{-2}/\text{Hz}^{1/2}$	$10^{-15} \text{ms}^{-2}/\text{Hz}^{1/2}$	$3 \times 10^{-15} \text{ms}^{-2}/\text{Hz}^{1/2}$
$\sqrt{S_x}$	$1.5 \times 10^{-11} \text{m}/\text{Hz}^{1/2}$	$10^{-12} \text{m}/\text{Hz}^{1/2}$	$8 \times 10^{-12} \text{m}/\text{Hz}^{1/2}$

TABLE I. Parameters of all three space based detectors.

to use for the four year mission lifetime are $A = 9 \times 10^{-45}$, $\alpha = 0.138$, $\beta = -221$, $\kappa = 521$, $\gamma = 1680$, and $f_k = 0.0013$ [57].

We show the root sensitivity curve for LISA, TianQin and TaiJi in Fig. 1, from which we can see that the sensitivity value of TianQin is higher than that of LISA in the frequency range $f \lesssim 0.01\text{Hz}$ and the sensitivity value of TianQin can be higher than Taiji when $f \lesssim 0.04\text{Hz}$. For the rest regions of frequency respectively, the LISA and TaiJi have higher sensitivity than that of TianQin, which suggests that comparing to TianQin, LISA and TaiJi are better for gravitational wave detections at lower frequencies (usually corresponds to higher black hole mass), while for higher frequencies we should turn to count on TianQin. In addition, we can see that the sensitivity of TaiJi is always lower than that of LISA in the whole frequency band which implies that TaiJi can be more sensitive to detect the gravitational wave signals emitted from the same source when compared with LISA.

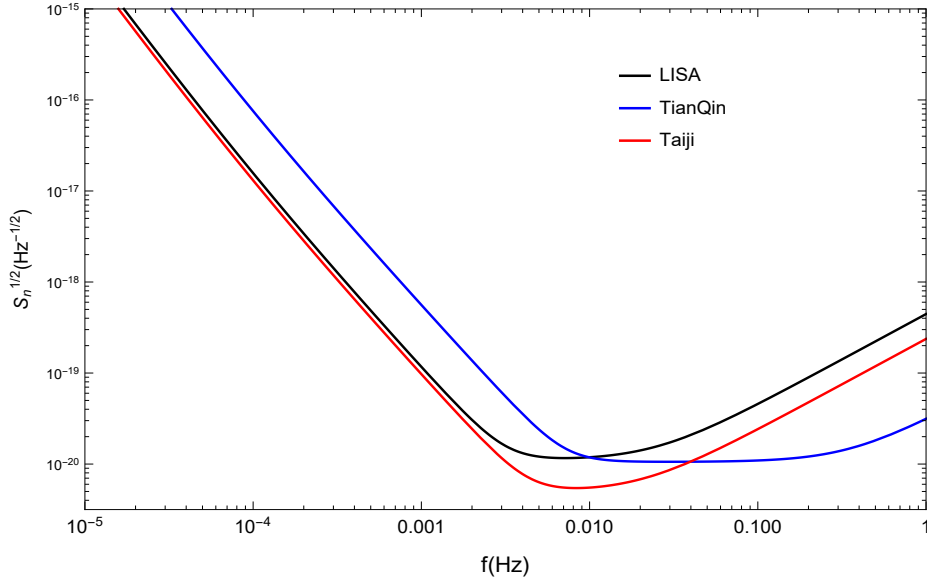


FIG. 1. The root sensitivity curves for LISA, TianQin and TaiJi.

III. SNR FOR NON-SINGULAR BHS IN CONFORMAL GRAVITY

A. Quasinormal modes of non-singular BHs in conformal gravity

The metric of non-singular BHs in conformal gravity can be expressed as [63]

$$ds^2 = S(r)ds_{\text{Schw}}^2 = -S(r)f(r)dt^2 + \frac{S(r)}{f(r)}dr^2 + S(r)r^2d\Omega^2, \quad (15)$$

where ds_{Schw}^2 is the Schwarzschild spacetime line element, with $f(r) = 1 - 2M/r$, the factor $S(r)$ is [63]

$$S(r) = \left(1 + \frac{L^2}{r^2}\right)^{2N}, \quad (16)$$

and N is an arbitrary positive integer and L is a new length scale. The additional conformal factor $S(r)$ making the spacetime singularity-free distinguishes the metric (15) from the Schwarzschild metric, and the metric (15) can reduce to Schwarzschild form when $S(r) \rightarrow 1$, i.e. $N \rightarrow 0$ or $L \rightarrow 0$. We will show that the non-zero parameters N, L will influence the dynamical behavior reflected by QNMs of BHs under gravitational perturbations. Since QNMs can disclose the black hole fingerprint, it can differentiate such non-singular BHs from the Schwarzschild black hole, as we will discuss in the following.

The master equation for the axial gravitational perturbation reads [64]

$$\frac{d^2 H^{(-)}}{dr_*^2} + (\omega^2 - V(r))H^{(-)} = 0, \quad (17)$$

where we have used tortoise radius defined by $dr/dr_* = f(r)$, $H^{(-)}$ is the radial part of the axial gravitational perturbation, ω is the QNM frequency, the effective potential V is [64]

$$V(r) = f(r) \left\{ \frac{l(l+1)}{r^2} - \frac{2}{r^2} - Z \frac{d}{dr} \left(\frac{f(r)dZ/dr}{Z^2} \right) \right\}, \quad (18)$$

and $Z(r) = \sqrt{S(r)}r$.

In [64], the 6th order WKB method was adopted to compute the QNM of the non-singular black hole configuration. In our numerical computation, we employ the 13th order WKB approximation. In the study of gravitational perturbations in the Schwarzschild black hole [52], comparing with the accurate numerical result, it was found that the 13th order WKB is more precise than the 6th WKB approach. It was argued that the WKB approximation works in satisfactory accuracy in calculating the QNM once $l \gg n$ [65], while does not work well for high overtone modes. In [64] the discussion on the QNM was only limited to the

lowest QNM for the gravitational perturbation. Including the Pade approximation, it was observed that there is a great increase of accuracy in calculating the QNM by using the WKB approach, furthermore with averaging of the Pade approximation accurate calculations can be achieved not only in the lowest mode, but also for the overtone modes with slightly bigger n than l , however the numerical results are still not much reliable for $n \gg l$, even if the Pade approximation is included [52].

In our numerical computation, we employ the 13th order WKB approximation method with averaging of the Pade approximations [52] to calculate the QNMs of the axial gravitational perturbation on the background of non-singular BHs. We show our results in Tables II and III where we express the QNM frequency in a dimensionless variable $M\omega$.

In Table. II where we fix the parameter L , we find that with the increase of N both the real part representing the oscillation frequency and the magnitude of the imaginary part relating to the damping time of QNMs will increase, which implies that with the increase of the parameter N in the non-singular black hole in conformal gravity, the gravitational perturbation can have more oscillations but die out faster. Comparing to the non-singular black hole backgrounds, we find that the perturbation of the Schwarzschild black hole with $N = 0$ can last longer. Our result confirms that reported in [64] where they limited their discussion to a fixed angular index l . Since we have adopted the Pade approximation, we can accurately calculate QNMs for the change of n, l until $n = l$ (to keep numerical accuracy, $n > l$ is not considered in our discussion). In the Schwarzschild background, for the same overtone mode when the angular index l becomes higher, we observe that the real parts of frequency are always higher, while the imaginary part is higher for $n \leq 2$, but decreases when $n > 2$. However this property does not hold for non-singular BHs with $N \neq 0$. In non-singular holes, for the same overtone modes the higher angular number l always results in a higher real part of the frequency but smaller imaginary part of the frequency, which suggests that for the same overtone mode the perturbation with higher angular index may last longer for non-singular BHs while in the Schwarzschild black hole perturbation the mode $l = 2, n = 0$ is always the longest one.

In Table. III we present the frequencies of QNMs for a fixed N parameter. With the increase of L , the real part of QNMs monotonously increases while the imaginary part increases from $L = 0$ to $L = 2$ but then decreases continuously with the further increase of L . This behavior agrees to the result reported in [64] for a fixed angular index l . Employing

TABLE II. Quasinormal frequency $M\omega$ for non-singular BHs in conformal gravity for parameter $L = 2$.

l	n	$N = 0$	$N = 2$	$N = 5$	$N = 10$
2	0	0.373675 - 0.088964 <i>i</i>	0.409160 - 0.121392 <i>i</i>	0.715683 - 0.134492 <i>i</i>	1.372383 - 0.139325 <i>i</i>
	1	0.346827 - 0.273930 <i>i</i>	0.407758 - 0.370858 <i>i</i>	0.719270 - 0.403565 <i>i</i>	1.376117 - 0.417754 <i>i</i>
	2	0.299998 - 0.478098 <i>i</i>	0.414498 - 0.620991 <i>i</i>	0.727050 - 0.672962 <i>i</i>	1.383599 - 0.695444 <i>i</i>
3	0	0.599443 - 0.092703 <i>i</i>	0.620553 - 0.107015 <i>i</i>	0.855703 - 0.125041 <i>i</i>	1.450989 - 0.135461 <i>i</i>
	1	0.582643 - 0.281297 <i>i</i>	0.604412 - 0.331714 <i>i</i>	0.853220 - 0.377014 <i>i</i>	1.452762 - 0.406564 <i>i</i>
	2	0.551686 - 0.479087 <i>i</i>	0.589888 - 0.569715 <i>i</i>	0.851142 - 0.632531 <i>i</i>	1.456717 - 0.678002 <i>i</i>
	3	0.511943 - 0.690318 <i>i</i>	0.584544 - 0.815114 <i>i</i>	0.851857 - 0.890962 <i>i</i>	1.463341 - 0.949499 <i>i</i>
4	0	0.809178 - 0.094163 <i>i</i>	0.825032 - 0.102217 <i>i</i>	1.013367 - 0.117947 <i>i</i>	1.549660 - 0.131294 <i>i</i>
	1	0.796631 - 0.284334 <i>i</i>	0.810029 - 0.311229 <i>i</i>	1.007860 - 0.356078 <i>i</i>	1.549669 - 0.394338 <i>i</i>
	2	0.772709 - 0.479908 <i>i</i>	0.786423 - 0.534230 <i>i</i>	0.999971 - 0.599176 <i>i</i>	1.550292 - 0.658511 <i>i</i>
	3	0.739836 - 0.683924 <i>i</i>	0.766779 - 0.768643 <i>i</i>	0.992948 - 0.846952 <i>i</i>	1.552405 - 0.923937 <i>i</i>
	4	0.701514 - 0.898237 <i>i</i>	0.754662 - 1.007982 <i>i</i>	0.988570 - 1.097952 <i>i</i>	1.556748 - 1.190222 <i>i</i>
5	0	1.012295 - 0.094870 <i>i</i>	1.025096 - 0.100075 <i>i</i>	1.181610 - 0.112849 <i>i</i>	1.664843 - 0.127206 <i>i</i>
	1	1.002221 - 0.285817 <i>i</i>	1.013275 - 0.302492 <i>i</i>	1.174978 - 0.340491 <i>i</i>	1.663474 - 0.382215 <i>i</i>
	2	0.982695 - 0.480328 <i>i</i>	0.991012 - 0.512278 <i>i</i>	1.164029 - 0.573071 <i>i</i>	1.661378 - 0.638801 <i>i</i>
	3	0.955004 - 0.680556 <i>i</i>	0.963850 - 0.734449 <i>i</i>	1.152084 - 0.811398 <i>i</i>	1.659565 - 0.897424 <i>i</i>
	4	0.921081 - 0.888197 <i>i</i>	0.940140 - 0.967011 <i>i</i>	1.141652 - 1.054348 <i>i</i>	1.659055 - 1.157978 <i>i</i>
	5	0.883335 - 1.104182 <i>i</i>	0.840158 - 1.120908 <i>i</i>	1.133807 - 1.300278 <i>i</i>	1.660604 - 1.419940 <i>i</i>

the Pade approximation, we accurately calculated QNMs with our 13th WKB approach for different n, l even when $n = l$. Similar to the Schwarzschild black hole, for the non-singular BHs we find that for the same overtone modes, with the increase of the angular number l , the real part of the frequency increases. The absolute imaginary part of the frequency for non-singular BHs presents different behaviors from that of the Schwarzschild background when L is not big enough. For the same overtone mode, with the increase of the angular number l , the absolute imaginary part of the frequency for a non-singular black hole decreases instead of increasing as in the Schwarzschild background. This is consistent with the picture we

TABLE III. Quasinormal frequency $M\omega$ for non-singular BHs in conformal gravity for parameter $N = 2$.

l	n	$L = 0$	$L = 2$	$L = 5$	$L = 15$
2	0	0.373675 - 0.088964i	0.409161 - 0.121392i	0.500121 - 0.105834i	0.530178 - 0.094147i
	1	0.346827 - 0.273931i	0.407758 - 0.370858i	0.496880 - 0.317166i	0.514476 - 0.284905i
	2	0.299998 - 0.478098i	0.414498 - 0.620991i	0.489883 - 0.526622i	0.484316 - 0.483647i
3	0	0.599443 - 0.092703i	0.620553 - 0.107015i	0.686818 - 0.101541i	0.708826 - 0.094852i
	1	0.582643 - 0.281297i	0.604412 - 0.331714i	0.679594 - 0.305861i	0.696048 - 0.286379i
	2	0.551686 - 0.479087i	0.589888 - 0.569715i	0.667081 - 0.512816i	0.671468 - 0.483427i
	3	0.511943 - 0.690318i	0.584544 - 0.815114i	0.648889 - 0.720679i	0.637497 - 0.689529i
4	0	0.809178 - 0.094163i	0.825032 - 0.102217i	0.876184 - 0.099544i	0.893459 - 0.095293i
	1	0.796631 - 0.284334i	0.810029 - 0.311229i	0.868380 - 0.299798i	0.882860 - 0.287183i
	2	0.772709 - 0.479908i	0.786423 - 0.534230i	0.853993 - 0.502905i	0.862299 - 0.482970i
	3	0.739836 - 0.683924i	0.766779 - 0.768643i	0.834321 - 0.709301i	0.833181 - 0.685113i
	4	0.701514 - 0.898237i	0.754662 - 1.007982i	0.809681 - 0.918896i	0.797793 - 0.895593i
5	0	1.012295 - 0.094871i	1.025096 - 0.100075i	1.066719 - 0.098481i	1.080916 - 0.095562i
	1	1.002221 - 0.285817i	1.013275 - 0.302492i	1.059305 - 0.296361i	1.071930 - 0.287641i
	2	0.982695 - 0.480328i	0.991012 - 0.512278i	1.045228 - 0.496726i	1.054373 - 0.482565i
	3	0.955004 - 0.680556i	0.963851 - 0.734449i	1.025583 - 0.700485i	1.029119 - 0.682139i
	4	0.921081 - 0.888197i	0.940140 - 0.967011i	1.001235 - 0.907965i	0.997555 - 0.887945i
	5	0.883335 - 1.104182i	0.840158 - 1.120908i	0.972539 - 1.119446i	0.961550 - 1.101097i

learn from Table.II, for the same overtone mode the perturbation for a non-singular black hole with a larger angular index l may last longer, which is different from the case in the Schwarzschild background, where the fundamental mode $n = 0, l = 2$ always dominates. The result of changing L looks more complicated than that for the change of N given above. When $L = 15$, the QNM frequencies return to the similar behavior with the change of n, l to that in the Schwarzschild background. In this case, for the same overtone number, we can see that the real part of the frequency increases monotonously with the angular number l , while for $n \leq 1$ the imaginary part is higher for larger l , but for $n > 1$ it decreases when

increasing l .

Precise numerical results of the QNM frequencies for different (n, l) are useful to calculate the multi-mode SNR of this non-singular black hole. However in this work we will concentrate on the single-mode SNR. Different from the Schwarzschild black hole, it looks that in the non-singular black hole background the mode $n = 0, l = 2$ is not apparently the dominant mode. Instead, for the same overtone mode, the imaginary frequency for a bigger angular index implies that the perturbation may last longer in the non-singular black hole. However, we notice that in the limit $l \rightarrow \infty$, the effective potential $V(r) \approx f(r)l^2/r^2$, which reduces to that of Schwarzschild BHs, which makes it difficult to distinguish the modes between the non-singular black hole and the Schwarzschild black hole in the large l limit. In the face of complicated data, actually a criterion to determine the dominant mode was suggested in [66]. We can find the dominant mode by choosing $\min\{\sqrt{\omega_R^2 + \omega_I^2}\}$. Applying this criterion, we find that it is always the $n = 0, l = 2$ mode that serves the dominant mode in the perturbation, which holds also in the non-singular black hole. If we look at the relation Eq. (A5) between the GW amplitude \mathcal{A}_{lm} and the energy radiation efficiency ϵ_{rd} , the $n = 0, l = 2$ mode always has the strongest amplitude corresponding to more powerful energy in this mode. This further guarantees that the $n = 0, l = 2$ mode dominates in the perturbation in the non-singular black hole. Now we can compare the same dominant single-mode SNR for the non-singular black hole and the Schwarzschild black hole, which allows us to explore their imprints in GWs.

B. SNR by LISA, TianQin and TaiJi

In this subsection we calculate the SNR for LISA, TianQin and TaiJi by using the QNMs we have obtained for non-singular BHs in conformal gravity. We explore the SNR related to the dominant mode $n = 0, l = 2$ in both of the non-singular and Schwarzschild BHs. At first we would like to focus on the discussion of SNR for LISA, and then we will take TianQin and TaiJi into consideration for comparisons.

In Fig. 2 we show the SNR curve by fixing the parameter L , while changing the parameter N . We can see that with the increase of the mass, the SNR will grow, which implies that LISA is more sensitive to GW signals generated by BHs with greater mass. For the Schwarzschild black hole with $N = 0$, the SNR will reach the maximum when the black hole

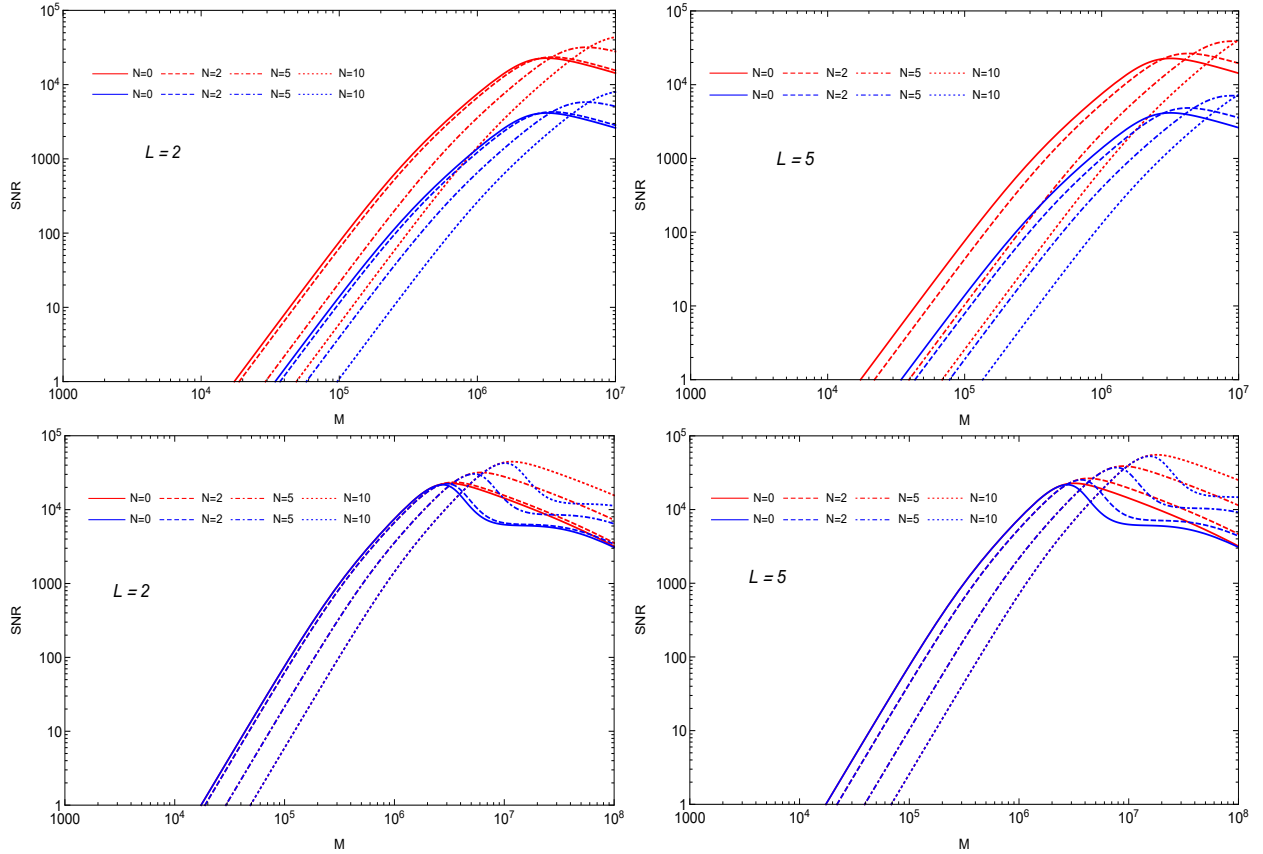


FIG. 2. The SNR behavior of LISA with the change of the black hole mass M at a distance $D_L = 3 \text{ Gpc}$, $z = 0.54$ with the angular number $l = 2$ in QNMs. For each plot we have fixed the value of L but changing N , and for the left two figures we set $L = 2$ and the right two figures we set $L = 5$. For the two plots in the top row the galactic noise is not considered, the red curves and blue curves correspond to the radiation efficiency $\epsilon_{rd} = 3\%$ and 0.1% , respectively, while for the two plots in the bottom we set $\epsilon_{rd} = 3\%$, and the red curves denote the SNR without including the galactic noise and the blue curves denote the SNR affected by the galactic noise.

mass becomes $\sim 10^6 M_\odot$. Thus for the Schwarzschild black hole LISA is most sensitive when the black hole mass is around $2 \times 10^6 M_\odot$. Considering the non-singular black hole with bigger N , we see that the SNR is smaller than that of the Schwarzschild black hole when the black hole mass is below $2 \times 10^6 M_\odot$ and with the increase of N , the SNR is more suppressed when the black hole mass is within this value. However when the black hole is more massive, the SNR of non-singular BHs catches up and exceeds further the value of the Schwarzschild black hole. We observe that a bigger N will have the maximum SNR appearing for more massive non-singular BHs. It is apparent that the bigger radiation efficiency ϵ_{rd} will lead to

the higher SNR as a natural result. In Fig. 3 we show the SNR at a fixed parameter N but with changing of the parameter L in each plot. The general feature in this case is similar to that illustrated in Fig. 2, the non-singular black hole has higher SNR when the black hole becomes more massive. Comparing Fig. 2 and Fig. 3, we observe that the SNR is more sensitive to the change of the parameter N than to the change of L . When the galactic confusion noise is taken into consideration (bottom rows) in Fig. 2 and Fig. 3, we see a dip appears when the black hole mass is a few times of $10^6 M_\odot$, for non-singular BHs with bigger L and N the dip starts to appear for more massive BHs. For smaller masses, the effect on SNR is negligible.

In Fig. 4 we show the effect of the angular index on the SNR for LISA. When the black hole mass is $\sim 10^6 M_\odot$, it is clear to see that the higher angular number always leads to a lower SNR because usually the signals with higher angular number are more subdominant in the energy distribution so that they result in smaller amplitudes. However, one may note that the maximum SNR for the larger angular number is higher when the black hole becomes more massive, which seems in contrast to our intuitions. This can be understood by the competition between the signals and noise. In the lower frequency region (corresponding to more massive BHs) we fix the black hole mass, and from Fig. 1 we can see that the noises which appear in the denominator in the SNR formula decreases with the increase of frequency related to the increase of the angular number of modes, while the strength of the signals which appear in the numerator is reduced with higher angular numbers, and this situation gives rise to the decrease of both signal strength and noise thus leading to the result that the modes with higher angular number will have higher SNR when BHs become very massive, as what we have demonstrated in Fig. 4. When the black hole becomes non-singular with bigger N , the difference in SNR caused by the angular index can be suppressed, which is just a direct consequence that the difference of the mode amplitudes among different angular numbers is reduced by increasing the parameter N .

In Fig. 5 we show a comparison of SNR among LISA, TianQin and TaiJi. From this figure one can see that there exists a maximal value of SNR for all these three detectors, and the mass related to the maximal SNR grows when the BHs deviate extensively from the Schwarzschild ones. It is clear to see that there exists a critical mass M_{cri} in each plot. For the mass range $M < M_{cri}$, the SNR for TianQin is higher than LISA implying that TianQin is more sensitive to GWs emitted from BHs with comparatively smaller masses, while for

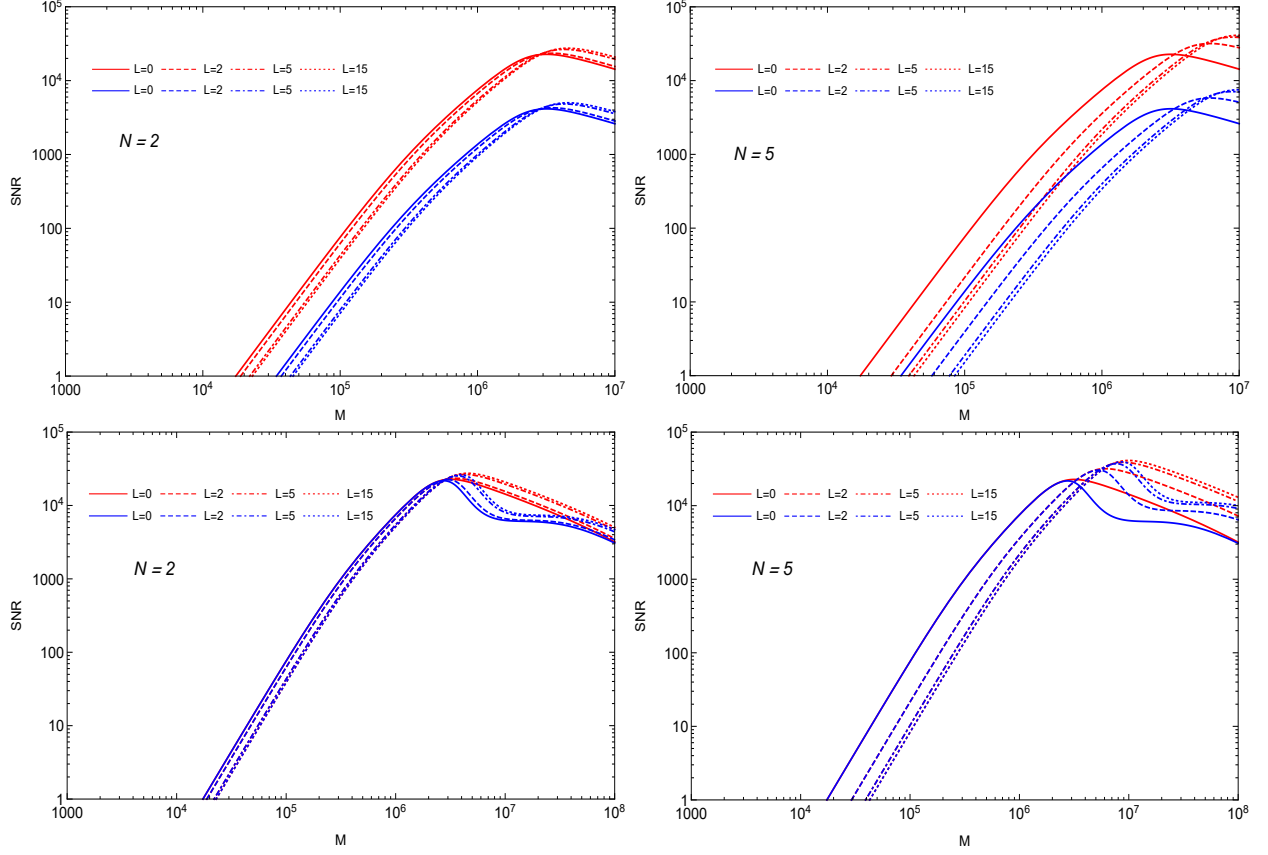


FIG. 3. The SNR behavior of LISA with the change of the black hole mass M at a distance $D_L = 3 \text{ Gpc}$, $z = 0.54$ with the angular number $l = 2$. For each plot we have fixed the value of N but change L , and for the left two figures we set $N = 2$ and the right two figures we set $N = 5$. For the two plots in the top row, the galactic noise is not included and the red curves and blue curves correspond to the radiation efficiency $\epsilon_{rd} = 3\%$ and 0.1% , respectively, while for the two plots in the bottom row we set $\epsilon_{rd} = 3\%$, and the red curves denote the SNR without including the galactic noise and the blue curves denote the SNR affected by the galactic noise.

more massive BHs with $M > M_{cri}$ the LISA and TaiJi is more sensitive for the detection. Different sensitivities of these three detectors were also reflected in the root sensitive curve shown in Fig. 1 which demonstrated that LISA and TaiJi are more sensitive to lower frequency (corresponding to bigger BHs) and TianQin is more sensitive to comparatively higher frequency GW signals (corresponding to smaller BHs). It is interesting to note that the critical mass M_{cri} is related to the parameter N , which increases when the black hole deviates more from the standard Schwarzschild black hole. It is noticeable that in the whole frequency band (from low frequency to high frequency) the SNR of TaiJi is higher

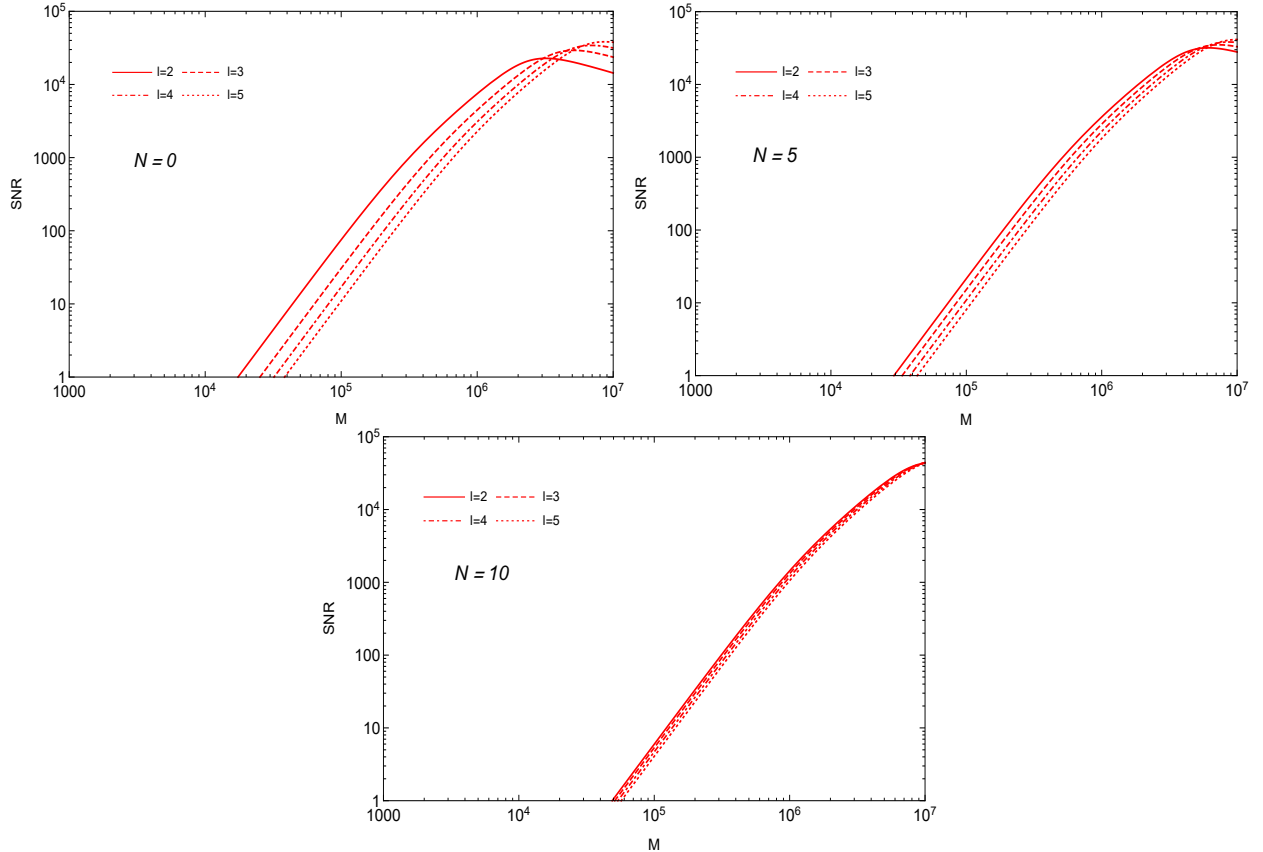


FIG. 4. The SNR of LISA for different angular numbers of l . The parameter L is set to be $L = 2$ in this figure, but 3 different N are assigned to each plot.

than LISA, which is consistent with the sensitivity demonstrated in Fig. 1. Comparing the values of M_{cri} and the locations of the dominant mode peaks of SNR for different non-singular parameters, LISA and TaiJi are more promising to distinguish non-singular BHs from the standard Schwarzschild ones.

IV. SNR FOR NON-SINGULAR BARDEEN BHs

A. Quasinormal modes of Bardeen BHs

The metric of the non-singular Bardeen black hole is [67]

$$ds^2 = -f(r)dt^2 + \frac{1}{f(r)}dr^2 + r^2(d\theta^2 + \sin^2\theta d\phi^2), \quad (19)$$

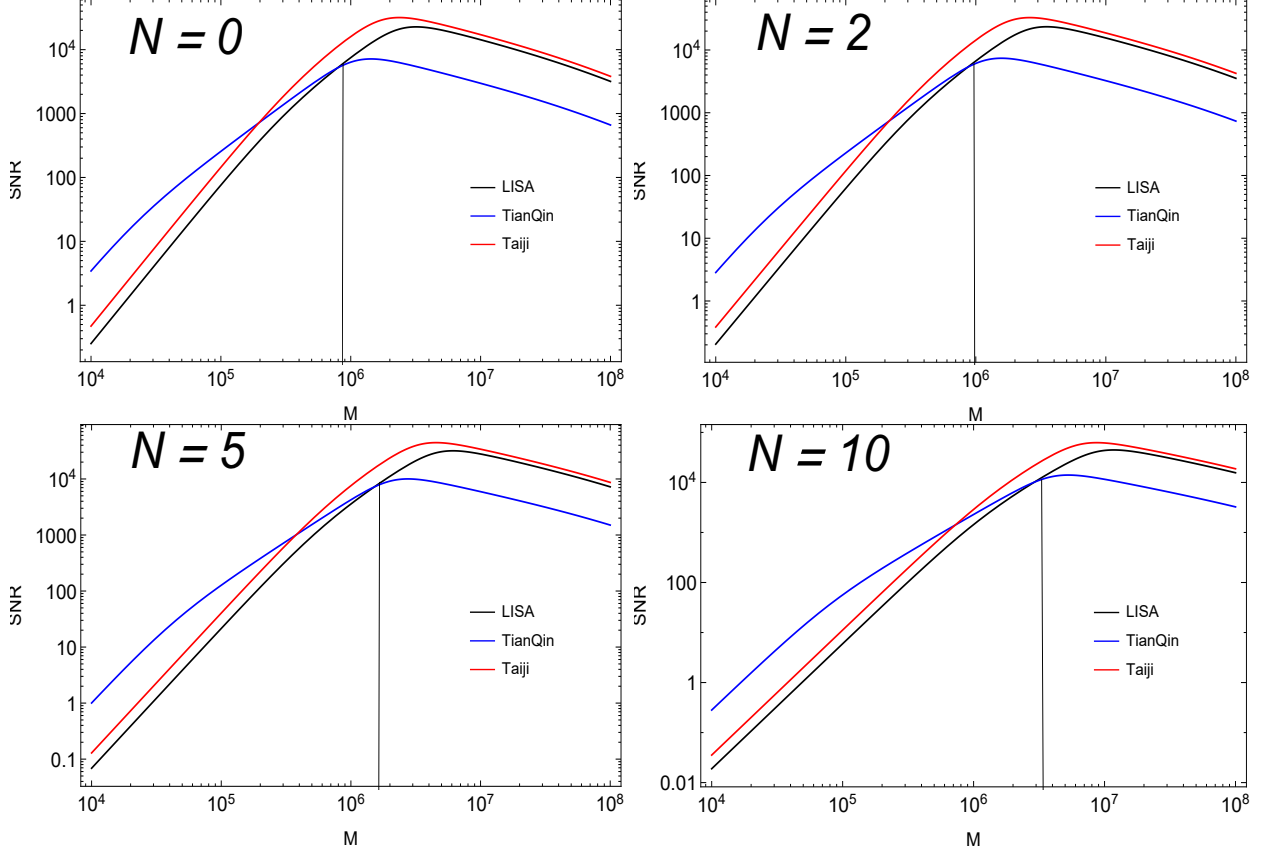


FIG. 5. The comparison of SNR among LISA, TianQin and Taiji with different black hole masses at a distance $D_L = 3 \text{ Gpc}$, $z = 0.54$ by taking the angular number $l = 2$ and the radiation efficiency $\epsilon_{rd} = 0.03$. In each plot we set $L = 2$, and four different N are designated correspondingly in the four plots.

where $f(r)$ is given by [67]

$$f(r) = 1 - \frac{2Mr^2}{(r^2 + \beta^2)^{\frac{3}{2}}}. \quad (20)$$

The parameter β can be regarded as the charge of a self-gravitating magnetic monopole system with mass M . To ensure the existence of BHs, the parameter β must be restricted to be $\beta^2 \leq \frac{16}{27}M^2$ and one can clearly see that when $\beta = 0$ the metric reduces to the Schwarzschild black hole. This parameter β makes the spacetime non-singular, which leads to different dynamical behaviors of the gravitational perturbation in contrast to that of the Schwarzschild black hole.

The master equation for the axial gravitational perturbation was given by [68]

$$\frac{d^2\phi}{dr_*^2} + [\omega^2 - V(r)]\phi = 0, \quad (21)$$

where the effective potential $V(r)$ reads

$$V(r) = f(r) \left(\frac{l(l+1) + 2(f(r) - 1)}{r^2} + \frac{1}{r} \frac{df(r)}{dr} + \frac{d^2f(r)}{dr^2} + 2\kappa L \right), \quad (22)$$

in which $\kappa = 8\pi$, and

$$L = \frac{3M}{|\beta|^3} \left(\frac{\sqrt{2\beta^2 F}}{1 + \sqrt{2\beta^2 F}} \right)^{\frac{5}{2}}, \quad F = \frac{\beta^2}{2r^4}. \quad (23)$$

In [68] the QNM was calculated by using the 3rd WKB method. It was found that compared with high order WKB approaches, the numerical result obtained by the 3rd WKB method is not very accurate [69]. In order to distinguish this non-singular black hole from the Schwarzschild black hole, we need very accurate results of the QNM spectrum. Therefore, in our calculations we will employ the 13th order WKB method and the Pade approximation to guarantee the high precision in our numerical computation.

We list our result in Table. IV. Analyzing the frequency of QNMs, we learn that with the increase of β , the real part of the QNM frequency increases for every fixed l, n mode, while the imaginary part of the perturbation frequency decreases for any given $l > 2$ with different n . Our result is different from that in [68], where it was claimed that the imaginary frequency keeps almost the same for different choices of β . This is because their 3rd WKB method is not accurate enough to show the details. Moreover in [68] the behavior of QNMs with the change of the angular number l is not discussed. With the Pade approximation, we are in a position to analyze carefully the dependence of the QNM frequency on the angular index l and the overtone number n until the limit $n \sim l$. With the increase of l at the same overtone number n , we find that both the real part and the imaginary part monotonously increase for $\beta = 0$ and $\beta = 0.3$ in the condition $n \leq 2$ and $n \leq 1$, respectively. For bigger β , for example $\beta = 0.6$, the imaginary part behaves differently. We have the spectrum of more accurate QNM frequencies for different modes. Hereafter we will focus on the calculation of single-mode SNR. For the complicated data, it is not easy to find the dominant mode in the gravitational perturbation. Here we will use again the criteria suggested in [66] by examining $\min\{\sqrt{\omega_R^2 + \omega_I^2}\}$, which tells us that the mode $n = 0, l = 2$ is dominant in both the non-singular and the Schwarzschild BHs. Taking into account that the $n = 0, l = 2$ mode always has the strongest amplitude \mathcal{A}_{lm} , it gives us further confidence to employ the $n = 0, l = 2$ mode to calculate the SNR in our following discussion.

TABLE IV. QNMs frequency $M\omega$ for non-singular Bardeen BHs.

l	n	$\beta = 0$	$\beta = 0.3$	$\beta = 0.6$
2	0	0.373675 - 0.088964 <i>i</i>	0.406175 - 0.087325 <i>i</i>	0.553008 - 0.094534 <i>i</i>
	1	0.346827 - 0.273931 <i>i</i>	0.381988 - 0.269701 <i>i</i>	0.525271 - 0.291523 <i>i</i>
	2	0.299998 - 0.478098 <i>i</i>	0.383018 - 0.475991 <i>i</i>	0.435513 - 0.485159 <i>i</i>
3	0	0.599443 - 0.092703 <i>i</i>	0.626872 - 0.091561 <i>i</i>	0.743159 - 0.089355 <i>i</i>
	1	0.582644 - 0.281297 <i>i</i>	0.612724 - 0.277584 <i>i</i>	0.731708 - 0.268568 <i>i</i>
	2	0.551686 - 0.479087 <i>i</i>	0.586992 - 0.471962 <i>i</i>	0.714495 - 0.445970 <i>i</i>
	3	0.511943 - 0.690318 <i>i</i>	0.692611 - 0.523967 <i>i</i>	0.692336 - 0.618884 <i>i</i>
4	0	0.809178 - 0.094163 <i>i</i>	0.835574 - 0.093074 <i>i</i>	0.942654 - 0.088437 <i>i</i>
	1	0.796631 - 0.284334 <i>i</i>	0.824486 - 0.280904 <i>i</i>	0.934782 - 0.266149 <i>i</i>
	2	0.772709 - 0.479908 <i>i</i>	0.803399 - 0.473636 <i>i</i>	0.919857 - 0.446242 <i>i</i>
	3	0.739836 - 0.683924 <i>i</i>	0.774487 - 0.673961 <i>i</i>	0.899410 - 0.630009 <i>i</i>
	4	0.701514 - 0.898237 <i>i</i>	0.740946 - 0.883478 <i>i</i>	0.876439 - 0.818826 <i>i</i>
5	0	1.012295 - 0.094871 <i>i</i>	1.039250 - 0.093792 <i>i</i>	1.145670 - 0.088485 <i>i</i>
	1	1.002221 - 0.285817 <i>i</i>	1.030170 - 0.282482 <i>i</i>	1.139280 - 0.266113 <i>i</i>
	2	0.982695 - 0.480328 <i>i</i>	1.012590 - 0.474430 <i>i</i>	1.126900 - 0.445668 <i>i</i>
	3	0.955004 - 0.680556 <i>i</i>	0.987689 - 0.671579 <i>i</i>	1.109250 - 0.628267 <i>i</i>
	4	0.921081 - 0.888197 <i>i</i>	0.957252 - 0.875455 <i>i</i>	1.087490 - 0.814877 <i>i</i>
	5	0.883335 - 1.104182 <i>i</i>	0.923566 - 1.086900 <i>i</i>	1.062670 - 1.005600 <i>i</i>

B. SNR by LISA, TianQin and TaiJi

Following the discussion in Section III, here we are going to discuss the SNR of the GW signal to be detected by LISA for non-singular Bardeen BHs at first, and then we will make a comparison of SNR among different space GW detectors, such as LISA, TianQin and TaiJi. For the non-singular Bardeen black hole and the Schwarzschild black hole having the same dominant mode, it is easy to compare their single-mode SNR.

We show the SNR curves for the Bardeen BHs with three different values, $\beta = 0$, $\beta = 0.3$ and $\beta = 0.6$ in Fig. 6. In the left panel we do not consider the galactic noise, while in

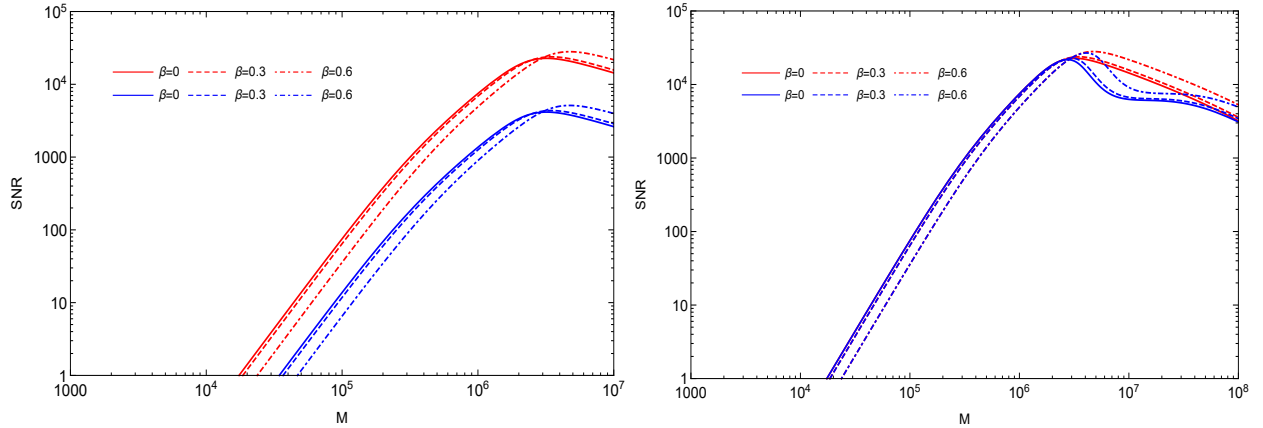


FIG. 6. The SNR behavior of LISA with the change of the black hole mass M at a distance $D_L = 3 \text{ Gpc}$, $z = 0.54$ when the angular index is taken $l = 2$. For the left plot, the red curves and blue curves correspond to radiation efficiency $\epsilon_{rd} = 3\%$ and 0.1% , respectively. For the right plot, we set $\epsilon_{rd} = 3\%$ and consider the comparison between SNR affected by the galactic noise (marked by blue lines) and SNR without including the galactic noise (marked by red curves).

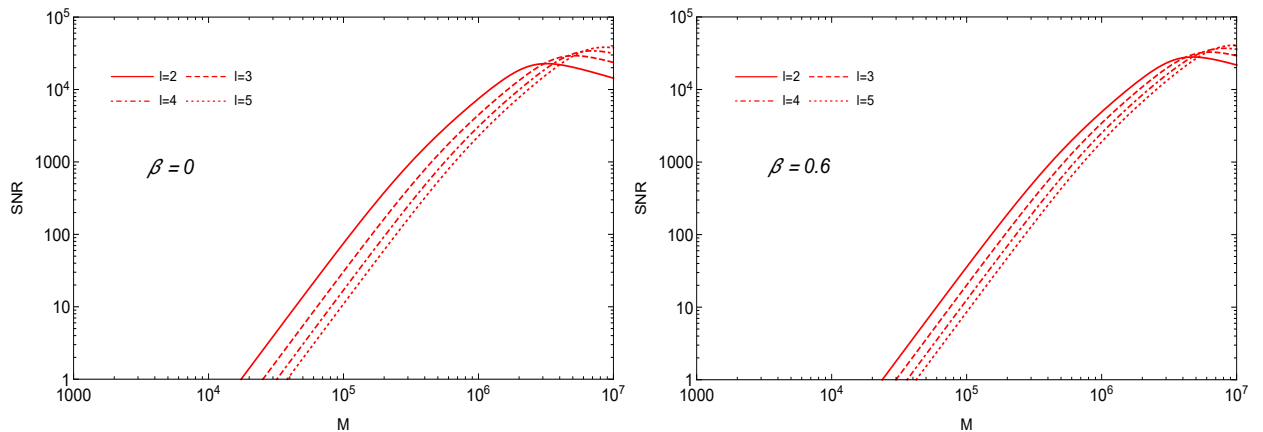


FIG. 7. SNR of LISA for different angular numbers l for the Bardeen black hole with the parameter $\beta = 0$ and $\beta = 0, 6$, respectively.

the right panel the noise is included. The general property of the SNR in this case is quite similar to that reported above for the non-singular conformal BHs in Section III. When the black hole mass $M < 2 \times 10^6 M_\odot$, the SNR for the Schwarzschild BHs with $\beta = 0$ is higher than that of the non-singular Bardeen BHs with a non-zero β . However for more massive BHs, the SNR for the non-singular Bardeen black hole exhibits higher peaks for bigger β . In Fig. 7 we demonstrate the effect of the angular index on the SNR for the Bardeen BHs

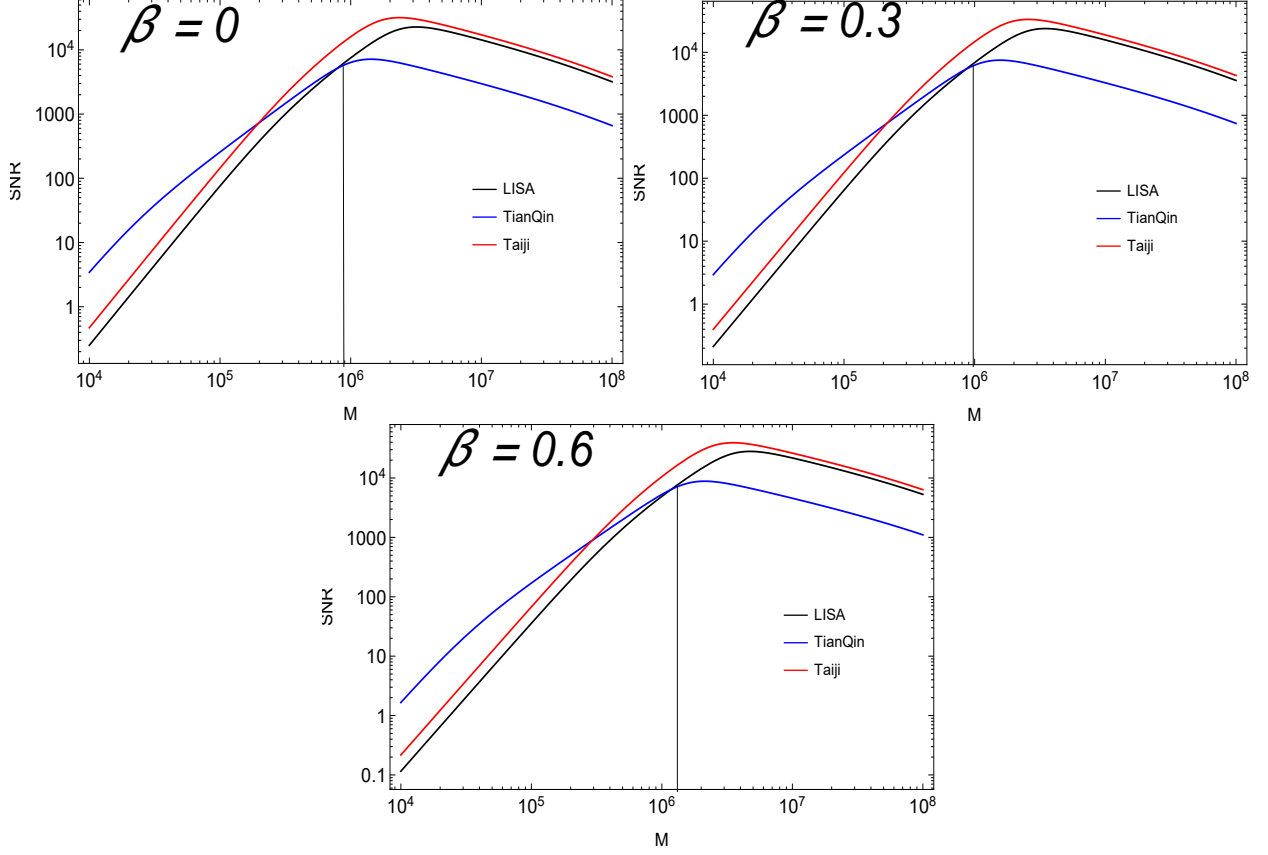


FIG. 8. The comparison of SNR among LISA and TianQin and TaiJi for the Bardeen BHs.

with $\beta = 0$ and $\beta = 0.6$. Similar to the case for conformal BHs in Section III, we find that higher l will accommodate higher SNR when the black hole becomes very massive. But this l influence on the SNR will be smoothed out by the increase of β .

In Fig. 8 we illustrate the comparison of SNR among LISA, TianQin and TaiJi. The comparison shows that there exists a critical mass M_{crit} , below which TianQin is more sensitive to detect the GW signal, while above this value LISA or TaiJi will detect the signal more sensitively. This critical mass M_{crit} increases with the increase of the Bardeen factor β . In the whole frequency band, it is clear that TaiJi has higher SNR than LISA. Again comparing the values of M_{crit} and the locations of SNR peaks for different Bardeen factors, LISA and TaiJi have more potential to distinguish the Bardeen non-singular BHs from the Schwarzschild ones.

V. CONCLUSIONS

In this paper we have calculated the quasinormal modes (QNMs) of the non-singular Bardeen BHs and singularity-free BHs in conformal gravity. We have also calculated their corresponding SNR in the single-mode waveform detection of GWs by the future space based interferometers, such as LISA, TianQin and TaiJi. We have found that the approximate formula (10) of SNR is not only valid for LISA, but also applicable to TianQin and TaiJi. Using this approach, we have calculated SNR for LISA, TianQin and TaiJi. We have investigated the impact of the conformal factor on the behavior of the SNR and found that the increase of the conformal factor will lead to a higher SNR for more massive BHs. For the Bardeen BHs, similar phenomena are also observed that a bigger Bardeen parameter β will result in a higher SNR, when the Bardeen black hole is very massive. Once the black hole mass is $\sim 10^6 M_\odot$, usually the GW perturbation in the Schwarzschild black hole has higher SNR and the non-singular modification cannot show up. The signature of the non-singular modification will emerge when BHs become more massive. Comparing the SNRs among LISA, TianQin and TaiJi, we found that the SNR of TianQin is always higher than that of LISA and TaiJi when the black hole is not so massive. However for the black hole with mass over a critical mass, LISA and TaiJi will have stronger SNR compared to that of TianQin. Interestingly, this critical mass increases when the black hole deviates significantly from the Schwarzschild black hole. In our study, we have found that the effect of the galactic confusion noise is not negligible, and its influence on the Schwarzschild black hole appears when the black hole mass is a few times of $10^6 M_\odot$, but for non-singular BHs the effect of the galactic noise will play an important role only for more massive holes. For the non-singular BHs, considering that their SNR peaks and dips appear for more massive BHs, it is expected that the LISA and TaiJi have more potential to distinguish them from the Schwarzschild black hole.

We have only studied the SNR for the single mode detection in this paper, and it is worth extending the discussion to multi-mode detections and making parameter estimation with the detected ringdown signals. For the multi-mode discussion, we have provided very accurate QNM frequency samples, which contain important properties for non-singular BHs. Besides we have only concentrated on BHs without angular momenta. Considering that BHs with rotation are more realistic in the universe, so it would be very interesting to generalize

our investigations to probe QNMs and SNR for rotating non-singular BHs.

ACKNOWLEDGMENTS

This research was supported in part by the National Natural Science Foundation of China, and the Major Program of the National Natural Science Foundation of China under Grant No. 11690021.

Appendix A: The approximation formula of SNR for TianQin and TaiJi

Although the approximate formula of SNR given by Eq. (10) from Ref. [54] was mainly developed in the context of LISA and the process of deriving Eq. (10) is dependent on the detector characteristics, the authors in Ref. [54] claimed that the expressions used in the derivation are valid for any interferometric detectors. To prove this claim, we calculate the SNR by using Eq. (10) for four QNMs in the Kerr BHs with $(l, m) = \{(2, 1), (2, 2), (3, 3), (4, 4)\}$ considered in Ref. [70], and compare the SNR of TianQin and TaiJi calculated by doing the full integral with the formula of SNR, given by Eq. (6a).

TABLE V. Fitting coefficients given by Ref. [54]

(l, m)	$f_1(l, m)$	$f_2(l, m)$	$f_3(l, m)$	$q_1(l, m)$	$q_2(l, m)$	$q_3(l, m)$
(2, 1)	0.6000	-0.2339	0.4175	-0.3000	2.3561	-0.2277
(2, 2)	1.5251	-1.1568	0.1292	0.7000	1.4187	-0.4990
(3, 3)	1.8956	-1.3043	0.1818	0.9000	2.3430	-0.4810
(4, 4)	2.3000	-1.5056	0.2244	1.1929	3.1191	-0.4825

The fitting formulae of the oscillation frequency ω_{lm} and damping time τ_{lm} for the remnant Kerr black hole with the redshifted mass $M_z = (1 + z)M$ are given by [54]

$$\omega_{lm} = \frac{f_1(l, m) + f_2(l, m)(1 - \chi_f)^{f_3(l, m)}}{M_z}, \quad (\text{A1a})$$

$$\tau_{lm} = \frac{2(q_1(l, m) + q_2(l, m)(1 - \chi_f)^{q_3(l, m)})}{\omega_{lm}}, \quad (\text{A1b})$$

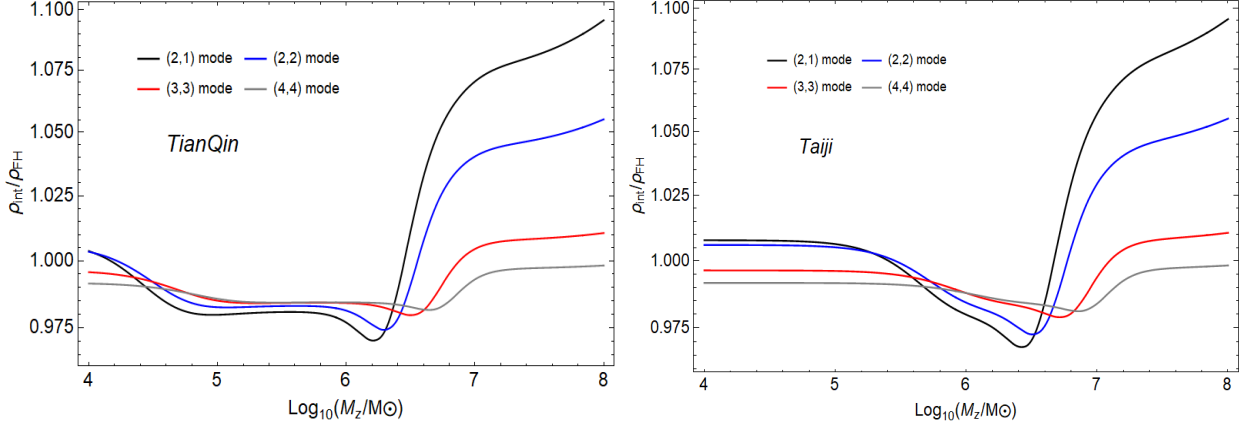


FIG. 9. The SNR ratio of ρ_{int} to ρ_{FH} . In this plot we take $\chi_f = 0.76$, $\chi_{eff} = 0.3$, $\nu = 2/9$ and luminosity distance $r = 15\text{Gpc}$.

where χ_f is the final spin parameter and the fitting coefficients are listed in Table. V. The amplitudes $\mathcal{A}_{lm}^+ = \mathcal{A}_{lm}^\times = \mathcal{A}_{lm}$ are given by [71, 72]

$$\mathcal{A}_{22}(\nu) = 0.864\nu, \quad (\text{A2a})$$

$$\mathcal{A}_{21}(\nu) = 0.43(\sqrt{1-4\nu} - \chi_{eff})\mathcal{A}_{22}(\nu), \quad (\text{A2b})$$

$$\mathcal{A}_{33}(\nu) = 0.44(1-4\nu)^{0.45}\mathcal{A}_{22}(\nu), \quad (\text{A2c})$$

$$\mathcal{A}_{44}(\nu) = (5.4(\nu-0.22)^2 + 0.04)\mathcal{A}_{22}(\nu), \quad (\text{A2d})$$

and

$$\nu = \frac{m_1 m_2}{(m_1 + m_2)^2}, \quad (\text{A3})$$

$$\chi_{eff} = \frac{1}{2} \left(\sqrt{1-4\nu}\chi_1 + \frac{m_1\chi_1 - m_2\chi_2}{m_1 + m_2} \right), \quad (\text{A4})$$

where (m_1, m_2) are the masses and (χ_1, χ_2) are the spin parameters of the original BHs. The energy radiation efficiency ϵ_{rd} appeared in Eq. (10) is related to the amplitude \mathcal{A}_{lm} by [54]

$$\mathcal{A}_{lm} = \sqrt{\frac{32Q_{lm}\epsilon_{rd}}{Mf_{lm}(1+4Q_{lm}^2)}}. \quad (\text{A5})$$

We have omitted the overtone index n in our expressions because only $n = 0$ modes are considered here. The SNR obtained by Eq. (6a) is denoted by ρ_{int} ,

$$\rho_{\text{int}}^2 = 4 \int_{f_{low}}^{f_{high}} \frac{|\tilde{h}_+|^2 + |\tilde{h}_\times|^2}{S_n(f)} df, \quad (\text{A6})$$

where f_{low} is taken to be the half of the (2,1) mode oscillation frequency and f_{high} is taken to be two times of the (4,4) mode frequency, and we also take the angle average $\langle |S_{lm}|^2 \rangle = 1/4\pi$ for all modes following the average made in Ref. [54]. Now we have calculated ρ_{FH} by adopting the approximate formula Eq. (10) and ρ_{int} obtained from the direct integral (A5) for comparison. In Fig. 9 we show the behavior of the ratio ρ_{int}/ρ_{FH} with the change of the black hole redshifted mass M_z for four different single QNMs. This figure shows that the value of ρ_{int} is close to ρ_{FH} , which suggests that the approximate formula Eq. (10) we have applied to calculate SNR for TianQin and TaiJi is feasible with acceptable errors in a single-mode wave detection.

-
- [1] LIGO SCIENTIFIC, VIRGO collaboration, B. P. Abbott et al., *Observation of Gravitational Waves from a Binary Black Hole Merger*, *Phys. Rev. Lett.* **116** (2016) 061102.
 - [2] LIGO SCIENTIFIC, VIRGO collaboration, B. P. Abbott et al., *GW151226: Observation of Gravitational Waves from a 22-Solar-Mass Binary Black Hole Coalescence*, *Phys. Rev. Lett.* **116** (2016) 241103.
 - [3] LIGO SCIENTIFIC, VIRGO collaboration, B. P. Abbott et al., *GW170608: Observation of a 19-solar-mass Binary Black Hole Coalescence*, *Astrophys. J.* **851** (2017) L35.
 - [4] LIGO SCIENTIFIC, VIRGO collaboration, B. P. Abbott et al., *GW170814: A Three-Detector Observation of Gravitational Waves from a Binary Black Hole Coalescence*, *Phys. Rev. Lett.* **119** (2017) 141101.
 - [5] LIGO SCIENTIFIC, VIRGO collaboration, B. P. Abbott et al., *Binary Black Hole Mergers in the first Advanced LIGO Observing Run*, *Phys. Rev.* **X6** (2016) 041015[erratum: *Phys. Rev.* **X8**,no.3,039903(2018)].
 - [6] LIGO SCIENTIFIC, VIRGO collaboration, B. P. Abbott et al., *GW170104: Observation of a 50-Solar-Mass Binary Black Hole Coalescence at Redshift 0.2*, *Phys. Rev. Lett.* **118** (2017) 221101[Erratum: *Phys. Rev. Lett.* **121**,no.12,129901(2018)].
 - [7] LIGO SCIENTIFIC, VIRGO collaboration, B. P. Abbott et al., *GW170817: Observation of Gravitational Waves from a Binary Neutron Star Inspiral*, *Phys. Rev. Lett.* **119** (2017) 161101.
 - [8] J. Kormendy and D. Richstone, *Inward bound—the search for supermassive black holes in*

- galactic nuclei, Annual Review of Astronomy and Astrophysics* **33** (1995) 581.
- [9] Y.-M. Hu, J. Mei and J. Luo, *Science prospects for space-borne gravitational-wave missions, National Science Review* **4** (2017) 683.
- [10] E. Barausse, J. Bellovary, E. Berti, K. Holley-Bockelmann, B. Farris, B. Sathyaprakash et al., *Massive Black Hole Science with eLISA, J. Phys. Conf. Ser.* **610** (2015) 012001.
- [11] A. Klein et al., *Science with the space-based interferometer eLISA: Supermassive black hole binaries, Phys. Rev.* **D93** (2016) 024003.
- [12] GRAVITY collaboration, R. Abuter et al., *Detection of the gravitational redshift in the orbit of the star S2 near the Galactic centre massive black hole, Astron. Astrophys.* **615** (2018) L15.
- [13] P. Amaro-Seoane, H. Audley, S. Babak, J. Baker, E. Barausse, P. Bender et al., *Laser interferometer space antenna, arXiv:1702.00786 [astro-ph.IM]* (2017) .
- [14] W.-R. Hu and Y.-L. Wu, *The Taiji Program in Space for gravitational wave physics and the nature of gravity, Natl. Sci. Rev.* **4** (2017) 685–686.
- [15] J. Luo, L.-S. Chen, H.-Z. Duan, Y.-G. Gong, S. Hu, J. Ji et al., *TianQin: a space-borne gravitational wave detector, Classical and Quantum Gravity* **33** (2016) 035010.
- [16] LIGO SCIENTIFIC, VIRGO, FERMI-GBM, INTEGRAL collaboration, B. P. Abbott et al., *Gravitational Waves and Gamma-rays from a Binary Neutron Star Merger: GW170817 and GRB 170817A, Astrophys. J.* **848** (2017) L13.
- [17] A. Goldstein et al., *An Ordinary Short Gamma-Ray Burst with Extraordinary Implications: Fermi-GBM Detection of GRB 170817A, Astrophys. J.* **848** (2017) L14.
- [18] I. Arcavi et al., *Optical emission from a kilonova following a gravitational-wave-detected neutron-star merger, Nature* **551** (2017) 64.
- [19] D. A. Coulter et al., *Swope Supernova Survey 2017a (SSS17a), the Optical Counterpart to a Gravitational Wave Source, Science* (2017) .
- [20] V. M. Lipunov et al., *MASTER Optical Detection of the First LIGO/Virgo Neutron Star Binary Merger GW170817, Astrophys. J.* **850** (2017) L1.
- [21] DES, DARK ENERGY CAMERA GW-EM collaboration, M. Soares-Santos et al., *The Electromagnetic Counterpart of the Binary Neutron Star Merger LIGO/Virgo GW170817. I. Discovery of the Optical Counterpart Using the Dark Energy Camera, Astrophys. J.* **848** (2017) L16.

- [22] N. R. Tanvir et al., *The Emergence of a Lanthanide-Rich Kilonova Following the Merger of Two Neutron Stars*, *Astrophys. J.* **848** (2017) L27.
- [23] S. Valenti, D. J. Sand, S. Yang, E. Cappellaro, L. Tartaglia, A. Corsi et al., *The discovery of the electromagnetic counterpart of GW170817: kilonova AT 2017gfo/DLT17ck*, *Astrophys. J.* **848** (2017) L24.
- [24] M. Shibata and K. Hotokezaka, *Merger and Mass Ejection of Neutron-Star Binaries*, *Ann. Rev. Nucl. Part. Sci.* **69** (2019) 41–64.
- [25] M. W. Coughlin, T. Dietrich, B. Margalit and B. D. Metzger, *Multimessenger Bayesian parameter inference of a binary neutron star merger*, *Mon. Not. Roy. Astron. Soc.* **489** (2019) L91–L96.
- [26] K. Kiuchi, K. Kyutoku, M. Shibata and K. Taniguchi, *Revisiting the lower bound on tidal deformability derived by AT 2017gfo*, *Astrophys. J.* **876** (2019) L31.
- [27] E. E. Flanagan and T. Hinderer, *Constraining neutron star tidal Love numbers with gravitational wave detectors*, *Phys. Rev.* **D77** (2008) 021502.
- [28] V. Cardoso, E. Franzin and P. Pani, *Is the gravitational-wave ringdown a probe of the event horizon?*, *Phys. Rev. Lett.* **116** (2016) 171101[Erratum: *Phys. Rev. Lett.*117,no.8,089902(2016)].
- [29] V. Cardoso, S. Hopper, C. F. B. Macedo, C. Palenzuela and P. Pani, *Gravitational-wave signatures of exotic compact objects and of quantum corrections at the horizon scale*, *Phys. Rev.* **D94** (2016) 084031.
- [30] J. Abedi, H. Dykaar and N. Afshordi, *Echoes from the Abyss: Tentative evidence for Planck-scale structure at black hole horizons*, *Phys. Rev.* **D96** (2017) 082004.
- [31] S. W. Hawking and R. Penrose, *The singularities of gravitational collapse and cosmology*, *Proc. R. Soc. Lond. A* **314** (1970) 529.
- [32] A. Ashtekar and M. Bojowald, *Quantum geometry and the Schwarzschild singularity*, *Class. Quant. Grav.* **23** (2006) 391–411.
- [33] P. Nicolini, A. Smailagic and E. Spallucci, *Noncommutative geometry inspired Schwarzschild black hole*, *Phys. Lett.* **B632** (2006) 547–551.
- [34] J. C. Lopez-Dominguez, O. Obregon, M. Sabido and C. Ramirez, *Towards Noncommutative Quantum Black Holes*, *Phys. Rev.* **D74** (2006) 084024.
- [35] S. Hossenfelder, L. Modesto and I. Premont-Schwarz, *A Model for non-singular black hole*

- collapse and evaporation, Phys. Rev. D* **81** (2010) 044036.
- [36] M. Bojowald, S. Brahma and D.-h. Yeom, *Effective line elements and black-hole models in canonical loop quantum gravity, Phys. Rev. D* **98** (2018) 046015.
- [37] A. Ashtekar, J. Olmedo and P. Singh, *Quantum Transfiguration of Kruskal Black Holes, Phys. Rev. Lett.* **121** (2018) 241301.
- [38] A. Ashtekar, J. Olmedo and P. Singh, *Quantum extension of the Kruskal spacetime, Phys. Rev. D* **98** (2018) 126003.
- [39] N. Bodendorfer, F. M. Mele and J. Münch, *Effective Quantum Extended Spacetime of Polymer Schwarzschild Black Hole, Class. Quant. Grav.* **36** (2019) 195015.
- [40] A. Ashtekar, *Black Hole evaporation: A Perspective from Loop Quantum Gravity, Universe* **6** (2020) 21.
- [41] K. Jusufi, M. Jamil, H. Chakrabarty, Q. Wu, C. Bambi and A. Wang, *Rotating regular black holes in conformal massive gravity, 1911.07520*.
- [42] S. Capozziello and M. De Laurentis, *Extended Theories of Gravity, Phys. Rept.* **509** (2011) 167–321.
- [43] E. Ayon-Beato and A. Garcia, *Regular black hole in general relativity coupled to nonlinear electrodynamics, Phys. Rev. Lett.* **80** (1998) 5056–5059.
- [44] F. Englert, C. Truffin and R. Gastmans, *Conformal Invariance in Quantum Gravity, Nucl. Phys.* **B117** (1976) 407.
- [45] G. 't Hooft, *A class of elementary particle models without any adjustable real parameters, Found. Phys.* **41** (2011) 1829–1856.
- [46] M. P. Dabrowski, J. Garecki and D. B. Blaschke, *Conformal transformations and conformal invariance in gravitation, Annalen Phys.* **18** (2009) 13–32.
- [47] P. D. Mannheim, *Making the Case for Conformal Gravity, Found. Phys.* **42** (2012) 388–420.
- [48] P. D. Mannheim, *Mass Generation, the Cosmological Constant Problem, Conformal Symmetry, and the Higgs Boson, Prog. Part. Nucl. Phys.* **94** (2017) 125–183.
- [49] L. Modesto and L. Rachwał, *Finite Conformal Quantum Gravity and Nonsingular Spacetimes, arXiv:1605.04173 [hep-th]* (2016) .
- [50] C. Bambi, L. Modesto and L. Rachwał, *Spacetime completeness of non-singular black holes in conformal gravity, JCAP* **1705** (2017) 003.
- [51] R. A. Konoplya and A. Zhidenko, *Quasinormal modes of black holes: From astrophysics to*

- string theory*, *Rev. Mod. Phys.* **83** (2011) 793–836.
- [52] J. Matyjasek and M. Opala, *Quasinormal modes of black holes. The improved semianalytic approach*, *Phys. Rev.* **D96** (2017) 024011.
- [53] R. A. Konoplya, A. Zhidenko and A. F. Zinhailo, *Higher order WKB formula for quasinormal modes and grey-body factors: recipes for quick and accurate calculations*, *Class. Quant. Grav.* **36** (2019) 155002.
- [54] E. Berti, V. Cardoso and C. M. Will, *Gravitational-wave spectroscopy of massive black holes with the space interferometer LISA*, *Phys. Rev. D* **73** (Mar, 2006) 064030.
- [55] E. Berti, V. Cardoso and A. O. Starinets, *Quasinormal modes of black holes and black branes*, *Class. Quant. Grav.* **26** (2009) 163001.
- [56] S.A.Teukolsky, *Pertubations of a rotation black hole.II. Dynamical stability of the kerr metric*, *Astrophys.J.* **185** (1973) 635.
- [57] T. Robson, N. J. Cornish and C. Liug, *The construction and use of LISA sensitivity curves*, *Class. Quant. Grav.* **36** (2019) 105011.
- [58] S. L. Larson, W. A. Hiscock and R. W. Hellings, *Sensitivity curves for spaceborne gravitational wave interferometers*, *Phys. Rev. D* **62** (2000) 062001.
- [59] D. Liang, Y. Gong, A. J. Weinstein, C. Zhang and C. Zhang, *Frequency response of space-based interferometric gravitational-wave detectors*, *Phys. Rev.* **D99** (2019) .
- [60] E. E. Flanagan and S. A. Hughes, *Measuring gravitational waves from binary black hole coalescences: 1. Signal-to-noise for inspiral, merger, and ringdown*, *Phys. Rev.* **D57** (1998) 4535–4565.
- [61] N. J. Cornish and S. L. Larson, *Space missions to detect the cosmic gravitational wave background*, *Class. Quant. Grav.* **18** (2001) 3473.
- [62] N. Cornish and T. Robson, *Galactic binary science with the new LISA design*, *Journal of Physics: Conference Series* **840** (2017) 012024.
- [63] C. Bambi, L. Modesto and L. Rachwał, *Spacetime completeness of non-singular black holes in conformal gravity*, *JCAP* **1705** (2017) 003.
- [64] C.-Y. Chen and P. Chen, *Gravitational perturbations of nonsingular black holes in conformal gravity*, *Phys. Rev.D* **99** (2019) 104003.
- [65] S. Iyer and C. M. Will, *Black Hole Normal Modes: A WKB Approach. 1. Foundations and Application of a Higher Order WKB Analysis of Potential Barrier Scattering*, *Phys. Rev.*

D35 (1987) .

- [66] B. Wang, C.-Y. Lin and C. Molina, *Quasinormal behavior of massless scalar field perturbation in Reissner-Nordstrom anti-de Sitter spacetimes*, *Phys. Rev.* **D70** (2004) 064025.
- [67] J. Bardeen, *Proceedings of GR5, Tiflis, U.S.S.R.*, 1968.
- [68] S. C. Ulhoa, *On Quasinormal Modes for Gravitational Perturbations of Bardeen Black Hole*, *Braz. J. Phys.* **44** (2014) 380.
- [69] R. A. Konoplya, *Quasinormal behavior of the d-dimensional Schwarzschild black hole and higher order WKB approach*, *Phys. Rev.* **D68** (2003) 024018.
- [70] C. Shi, J. Bao, H.-T. Wang, J.-d. Zhang, Y.-M. Hu, A. Sesana et al., *Science with the tianqin observatory: Preliminary results on testing the no-hair theorem with ringdown signals*, *Phys. Rev. D* **100** (2019) 044036.
- [71] I. Kamaretsos, M. Hannam and B. S. Sathyaprakash, *Is black-hole ringdown a memory of its progenitor?*, *Phys. Rev. Lett.* **109** (2012) 141102.
- [72] J. Meidam, M. Agathos, C. Van Den Broeck, J. Veitch and B. S. Sathyaprakash, *Testing the no-hair theorem with black hole ringdowns using tiger*, *Phys. Rev. D* **90** (2014) 064009.